Journal of Power Sources 196 (2011) 8858–8865

Contents lists available at ScienceDirect

Journal of Power Sources

journal homepage: www.elsevier.com/locate/jpowsour

Enhancement of the energy storage properties of supercapacitors using graphene nanosheets dispersed with metal oxide-loaded carbon nanotubes

R.B. Rakhi, H.N. Alshareef*

Material Science and Engineering, King Abdullah University of Science and Technology, Thuwal 23955-6900, Saudi Arabia

ARTICLE INFO

Article history:
Received 14 January 2011
Received in revised form 7 April 2011
Accepted 7 June 2011
Available online 15 June 2011

Keywords:
Supercapacitor
Graphene nanosheets
SnO_2 loaded MWCNTs, Specific capacitance, Energy density, Power density, Cycle life

ABSTRACT

Graphene nanosheets (GNs) dispersed with SnO_2 nanoparticles loaded multiwalled carbon nanotubes (SnO_2–MWCNTs) were investigated as electrode materials for supercapacitors. SnO_2–MWCNTs were obtained by a chemical method followed by calcination. GNs/SnO_2–MWCNTs nanocomposites were prepared by ultrasonication of the GNs and SnO_2–MWCNTs. Electrochemical double layer capacitors were fabricated using the composite as the electrode material and aqueous KOH as the electrolyte. Electrochemical performance of the composite electrodes were compared to that of pure GNs electrodes and the results are discussed. Electrochemical measurements show that the maximum specific capacitance, power density and energy density obtained for supercapacitor using GNs/SnO_2–MWCNTs nanocomposite electrodes were respectively 224 F g^{-1}, 17.6 kW kg^{-1} and 31 Wh kg^{-1}. The fabricated supercapacitor device exhibited excellent cycle life with ~81% of the initial specific capacitance retained after 6000 cycles. The results suggest that the hybrid composite is a promising supercapacitor electrode material.

1. Introduction

Electrochemical capacitors (ECs) or supercapacitors are energy-storage devices which possess higher energy density (0.5–10 Wh kg^{-1}) than conventional dielectric capacitors and higher power density (1–10 kW kg^{-1}) than batteries [1]. Moreover, they have high cycling ability and light mass, which make them promising energy storage devices of the future. ECs find applications in electric vehicles, uninterruptible power supplies, DC power systems, and mobile devices [2]. A supercapacitor stores energy using either ion adsorption (electrical double layer capacitors, EDLCs) or fast and reversible Faradic reactions (pseudocapacitors) [3]. These two mechanisms can function simultaneously, depending on the nature of the electrode material. While EDLCs, the most common supercapacitors at present, use carbon-based active materials with high surface area as the electrode materials, pseudocapacitors use transition metal oxides or electrically conducting polymers as active materials [4]. Hybrids of carbon materials and pseudocapacitor materials are reported to give superior performance as compared to their individual counterparts [5].

In the last few years, graphene, by virtue of its unique structure of two-dimensional layered hexagonal lattice of carbon atoms has attracted significant research interest as a potential electrode material for electrochemical energy storage [6]. The excellent properties that make graphene unique for electrode materials are high mobility, remarkable mechanical stiffness, high surface area and excellent conductivity [7,8]. Use of thermally exfoliated graphene nanosheets (GNs) as supercapacitor electrode materials has been reported to give a maximum specific capacitance of 117 F g^{-1} in aq. H_2SO4 electrolyte [9]. For supercapacitors made of chemically modified GNs, a specific capacitance of 135 F g^{-1} in aqueous KOH electrolyte has been reported [10]. Fabrication and performance studies of symmetric super capacitors based on curved GNs electrodes, capable of operation at a high voltage (4 V) in ionic liquid electrolyte 1-ethyl-3-methylimidazolium tetrafluoroborate with an exceptional high energy density of 85.6 Wh kg^{-1} at 1 A g^{-1} has also been reported [6]. Irreversible agglomeration and restacking of GNs due to van der Waals interactions, to form graphite during the drying process during electrode preparation is a major problem faced in graphene based supercapacitors. The agglomeration adversely affects supercapacitor performance by preventing electrolyte penetration into layers [11], and can be avoided by the introduction of spacers into the graphene layers. Both nanocarbon materials and pseudocapacitance materials have been used as spacers. Spacers ensure high electrochemical utilization of graphene layers as well as contribute to the total capacitance of the system [12]. The incorporation of carbon black (CB) into graphene has been reported to help in inhibiting the agglomeration of GNs and thereby improving the electrolyte–electrode accessibility as well as the electrode conductivity of supercapacitors [13]. Use of conducting polymer polyaniline (PANI) nanofibres as spacers to improve the supercapacitor performance of GNs has also been demonstrated

* Corresponding author. Tel.: +966 (0)2 808 4477; mobile: +966 (0)54 470 0037.
E-mail address: husam.alshareef@kaust.edu.sa (H.N. Alshareef).

0378-7753/$ – see front matter © 2011 Elsevier B.V. All rights reserved.
doi:10.1016/j.jpowsour.2011.06.038

[14,15]. Lack of long-term stability during cycling due to degradation of electroactive polymers is the major problem faced in the case of conducting polymers [4].

As compared to CB, carbon nanotubes (CNTs) have superior material properties such as high chemical stability, aspect ratio, mechanical strength and activated surface area and outstanding electrical properties, which make them widely accepted as supercapacitor electrode materials [16–20]. Theoretical estimation has been made on the effects of curvature upon the properties of the diffuse double layer at a charged CNT in electrolytic solution by solving Poisson–Boltzmann equation numerically in cylindrical space [20]. Various reports are available on the use of graphene/CNTs composites as supercapacitor electrodes [12,21]. Significant enhancement in electrochemical storage capacity has been observed in these composites with the existence of CNTs which are believed to bridge the defects for electron transfer and, in the mean time, to increase the basal spacing between graphene sheets [22]. Recently, Fan et al. reported the use of 3D CNT/graphene sandwich structures with CNT pillars grown in between the graphene layers by CVD approach as efficient electrodes in supercapacitors [21].

Enhancement in electrochemical performance of CNTs can be achieved by incorporation of either a metal oxide or a conducting polymer [18,19]. Significant improvement in the supercapacitor performance of GNs by dispersion of MWCNTs/PANI composites have been reported [23]. In a similar way, it is expected that a nanocomposite obtained by dispersion of transition metal oxide (TMO) nanoparticles loaded MWCNTs in GNs can serve as suitable electrode material for high performance super capacitors with an additional advantage of excellent cycling stability for practical applications. The use of hydrous RuO_2/GNs composites with different loadings of Ru as efficient supercapacitor electrodes with a maximum specific capacitance value of 570 F g^{-1} has been reported [24]. But, the commercial application of RuO_2 as electrode materials in supercapacitors has been restricted due to the high cost of Ru and because of this limitation, other cheap TMOs are currently being studied, as an alternative material for the RuO_2 [25–27].

Among the different TMOs for supercapacitor electrodes, SnO_2 is of particular interest due to its good chemical stability, high conductivity, ready availability, environmentally benign nature and lower cost as compared to the state-of-the-art electrode material RuO_2 [3]. There have been a variety of reports on the synthesis of SnO_2 nanoparticles by different methods like sol–gel synthesis, on mini arc plasma [28], hydrolysis of tin isopropoxide [29], chemical reduction of $SnCl_2$ followed by calcinations [30], from dendritic polymers [31], etc. Improvement of electrochemical energy storage properties of GNs based supercapacitors by direct deposition of SnO_2 nanoparticle has been reported [26,27,32]. As the electrochemical performance of SnO_2 nanoparticles largely depends on their microstructure and surface area, the development of controlled synthesis of SnO_2 nanostructures with high electroactive area is of great importance.

In the present work a new strategy to produce GNs dispersed with SnO_2 nanoparticles loaded MWCNTs composites (GNs/SnO_2–MWCNTs) as electrodes for ECs has been presented. The incorporation of SnO_2–MWCNTs into graphene layers is expected to improve electrolyte–electrode accessibility and electrode conductivity by reducing the agglomeration of GNs. SnO_2–MWCNTs composite is prepared by a simple chemical method. GNS/SnO_2–MWCNTs composite has been prepared by ultrasonication of GNs and SnO_2–MWCNTs. Supercapacitor devices are fabricated using GNs/SnO_2–MWCNTs nanocomposite electrode materials and performance studies are conducted. The electrochemical performance of the composite electrodes has been compared to that of pure GNs electrodes and the results are discussed.

2. Experimental

2.1. Synthesis of SnO_2–MWCNT composites

MWCNTs of purity 95% were functionalized by refluxing in conc. nitric acid (5N) at 60 °C for 4 h to make them more dispersible in deionized (DI) water. 10 mg of functionalized MWCNTs was dispersed in 40 ml of DI water by ultrasonication (Branson 3510) with subsequent addition of 1 ml of HCl (38%) and 1 g of hydrous $SnCl_2$. The mixture was sonicated for 5 min and then stirred for 60 min at room temperature. The precipitate was filtrated and washed completely using distilled water and then dried in air at 90 °C for 6 h. Part of the final product was calcined at 350 °C for 2 h.

2.2. Preparation of GNs/SnO_2–MWCNTs composites

The GNs/SnO_2–MWCNTs composite was synthesized by ultrasonication of chemically functionalized GNs and SnO_2–MWCNTs. In order to produce chemically functionalized graphene, 200 mg of few layered GNs (prepared using a procedure similar to that reported in [33]) was dispersed in 200 ml of concentrated acid mixture (nitricacid:sulphuric acid = 1:3) by continuous stirring at 80 °C for about 6 h. The resultant dispersion was filtered and washed several times with DI water. The filtrate was collected and dried in air without heating [33]. GNs and SnO_2–MWCNTs composites in the ratio 9:1 by weight were dispersed in 200 ml of distilled water by ultrasonication for 5 h to obtain a homogeneous GNs/SnO_2–MWCNTs suspension. Finally, the solid was filtered, and washed several times with distilled water and alcohol, dried at 100 °C for 12 h in a vacuum oven. An illustration of the preparation of GNs/SnO_2–MWCNTs composite is shown in Fig. 1.

2.3. General characterization of composites

The electrode materials were characterized by a powder X-ray diffraction system (XRD, Bruker, D8 ADVANCE) equipped with Cu K_α radiation (λ = 0.15406 nm). Raman spectroscopic measurements were carried out using a LabRam Aramis Raman spectrometer with He–Ne laser having an excitation wavelength of 633 nm. The surface morphology and microstructure of the samples were investigated by a scanning electron microscopy (SEM, FEI Helios NanoLab) and transition electron microscopy (TEM, FEI Titan).

2.4. Preparation of electrodes and electrochemical measurement

Circular supercapacitor electrodes, each with a diameter of 1.6 cm was prepared using GNs/SnO_2–MWCNTs composite material by the following procedure. The composite was mixed with polytetrafluoroethylene (PTFE) binder in a mass ratio of 95:5 and dispersed in ethanol. The resulting mixture was homogenized by ultrasonication and coated onto the conductive carbon cloth (ELAT, Nuvant systems Inc.) substrate, which was followed by drying at 100 °C for 12 h in a vacuum oven. Each electrode contained 4 mg of electroactive material and 0.2 mg of PTFE binder. Each supporting carbon cloth substrate was having a mass of 26 mg. Total mass of each electrode including the substrate mass was 30.2 mg. The two electrodes were separated by a thin polymer separator (Celgard® 3400) in 30 wt% KOH aqueous electrolyte and were sandwiched in a supercapacitor test cell (ECC-std, EL-Cell GmbH).

The electrochemical properties of the supercapacitor electrodes were studied in a two electrode configuration by cyclic voltammetry (CV), galvanostatic charge–discharge and electrochemical impedance spectroscopy (EIS) using a Modulab (Solartron Analytical) electrochemical workstation. The two electrode configuration is preferred as it provides the most reliable results of a material's performance for electrochemical capacitors. CV tests were carried

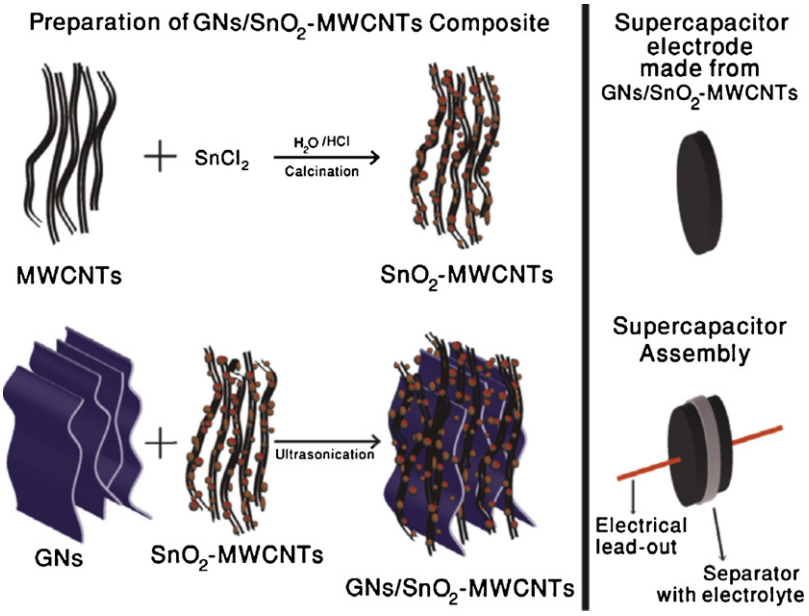

Fig. 1. Schematic of preparation of supercapacitor electrode material.

out in a potential range of −0.6 V to 0.5 V (vs. standard hydrogen electrode) at different scan rates varying from 5 mV s^{-1} to 200 mV s^{-1}. Galvanostatic charge–discharge measurements were carried out at different currents ranging from 5 mA to 50 mA, and EIS measurements were carried out in the frequency range from 100 kHz to 10 MHz at a dc bias of 0 V with a sinusoidal signal of 10 mV. EIS data was analyzed using complex plane impedance plots (Nyquist plots). Each data point in Nyquist plot is at a different frequency. Since the measurements are made on symmetric assemblies of materials, by the basic circuit relationship for series capacitors what is measured is actually 1/2 of the capacitance of the freestanding electrode [34]. The cell capacitance (C in F) was then calculated from the cyclic voltammograms (CVs) according to Eq. (1) or from the charge–discharge curves according to Eq. (2)

$$C = \frac{i}{f} \tag{1}$$

where 'i' is the average cathodic current of CV loop and 'f' is the scan rate [34].

$$C = \frac{I}{(\Delta V/\Delta t)} \tag{2}$$

where 'I' is the constant current for charge–discharge, $\Delta V/\Delta t$ is the slope of the discharge curve [34]. The specific capacitance (C_{sp} in F g^{-1}) was then calculated as

$$C_{sp} = \frac{2C}{m} \tag{3}$$

where 'm' is the mass of each electrode. In the present study, for specific capacitance calculation electrode mass was taken as 4 mg (mass of the active materials only).

3. Results and discussion

Powder XRD patterns of GNs, MWCNTs and SnO_2–MWCNTs are shown in Fig. 2. The XRD of GNs shows a peak at 26.4° corresponding to reflection from (0 0 2) plane of hexagonal graphite (JCPDS Card No. 75-1621). Whereas this reflection shifts to a lower 2θ value (25.9°) for MWCNTs. Shift in the 2θ value can be attributed to the structural difference of MWCNTs and GNs, since the hexagonal carbon sheets of MWCNTs have curved structure, whereas the graphene layers have planar structure. Thus, the interplanar d (0 0 2) spacing of MWCNTs is larger than graphene layers. For SnO_2–MWCNTs, peaks marked with an asterisk correspond to characteristic diffraction peaks from SnO_2 nanoparticles (JCPDS Card No. 41-1445). The graphitic peak at 2θ = 25.9° overlaps with the (1 1 0) peak from SnO_2. MWCNTs supply nucleation sites for the deposition of SnO_2 nanoparticles. A detailed explanation on the role of HCl addition in the formation of SnO_2-nanoparticles can be found in the work reported by Fang et al. [30]. The powder XRD pattern for SnO_2–MWCNTs is found to have large amount of background noise. SnO particles may also present in the composite, but they are not visible in the spectrum and the main peak of crystalline SnO corresponding to (1 0 1) plane (JCPDS Card No. 06-0395) is absent. This may be due to detection limitation or some structural change.

The formation of the SnO_2 nanoparticles are further confirmed from the Raman spectra (Fig. 3) of SnO_2–MWCNTs. Apart from the characteristic D and G bands of MWCNTs, the spectra contains additional peaks corresponding to vibrational modes of SnO_2 nanoparticles. The peaks at 480 cm^{-1}, 634 cm^{-1} and 776 cm^{-1} respectively corresponds to classical vibration modes E_g, A_{1g} and B_{2g} of SnO_2 nanoparticles while bands S_1 (576–568 cm^{-1}), S_2

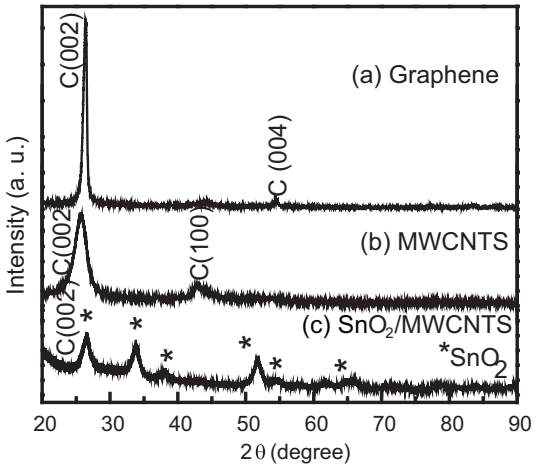

Fig. 2. Powder XRD of (a) GNs, (b) MWCNTs and (c) SnO_2–MWCNTs.

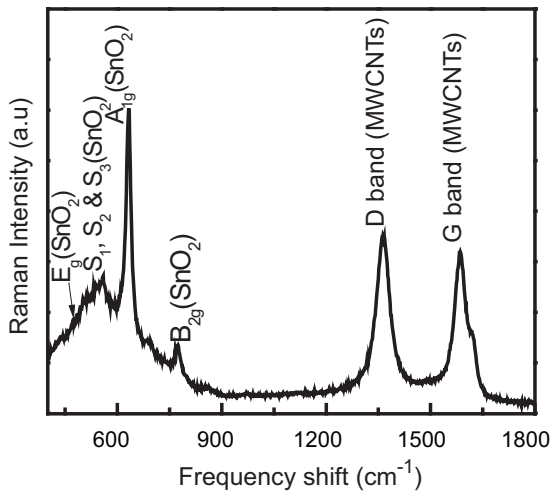

Fig. 3. Raman spectra of SnO_2–MWCNTs.

(542–486 cm^{-1}), and S_3 (691–707 cm^{-1}) appear as a consequence of disorder activation. Size of nanoparticle has got great influence on Raman spectra. The mode A_{1g} shifts to lower wave numbers as the nanoparticle size decreases. A detailed study of Raman shift as a function of SnO_2 nanoparticle size and fitting of the bands appearing in the high-frequency region of the Raman spectrum of a SnO_2 powder of very small grain size have been reported [35]. The Raman spectra obtained in the present study matches well with the literature data [35], indicating nanoparticles have an average diameter of 5–6 nm. High resolution TEM is also used as an additional tool for confirming the nanoparticle size.

TEM images of MWCNTs and SnO_2–MWCNTs are shown in Fig. 4(a) and (b) respectively. MWCNTs are having an average inner diameter of 10 nm and an outer diameter of 30 nm and are having an average length in the range of 10–30 μm. Fig. 4(b) suggests an uniform distribution of SnO_2 nanoparticles over the surface of MWCNTs. HRTEM image of SnO_2–MWCNTs (inset of Fig. 4(b)) reveals that the SnO_2 nanoparticles are highly crystalline in nature with an average particle size of 4–6 nm. This value matches very well with the value obtained from Raman spectra. TEM images of large area GNs and GNs/SnO_2–MWCNTs composite are shown in Fig. 4(c) and 4(d) respectively. SnO_2–MWCNTs are seen to occupy the surface of GNs.

Fig. 5(a) shows the SEM image of the carbon fabric which serves the purpose of the substrate for the deposition of the electrode material as well as current collector of the supercapacitor test cell. The carbon fabric substrate is a double layer structured gas diffusion layer porous carbon fabric made of macroporous layer of carbon fiber fabric (Nuvant systems Inc.) and a microporous layer of carbon black powder (inset of Fig. 5(a)) with a hydrophobic agent. The carbon black powder enhances an intimate electronic contact between the carbon based composite electrode material and the macroporous carbon fabric and can directly help in the reduction of internal resistance of the supercapacitor with the help of a well formed electrode electrolyte interface. SEM images of GNs uniformly coated onto the conductive carbon cloth substrate are shown in Fig. 5(b) and (c) while that of GNs/SnO_2–MWCNTs composite is shown in Fig. 5(d). Graphene layers interact with each other to form an open pore system, through which electrolyte ions easily access the surface of graphene to form electric double layers.

Fig. 6(a) and (b) respectively shows CV loops of the GNs and GNs/SnO_2–MWCNTs based symmetric supercapacitors. In the present study, supercapacitor devices retain rectangular CV loops, which

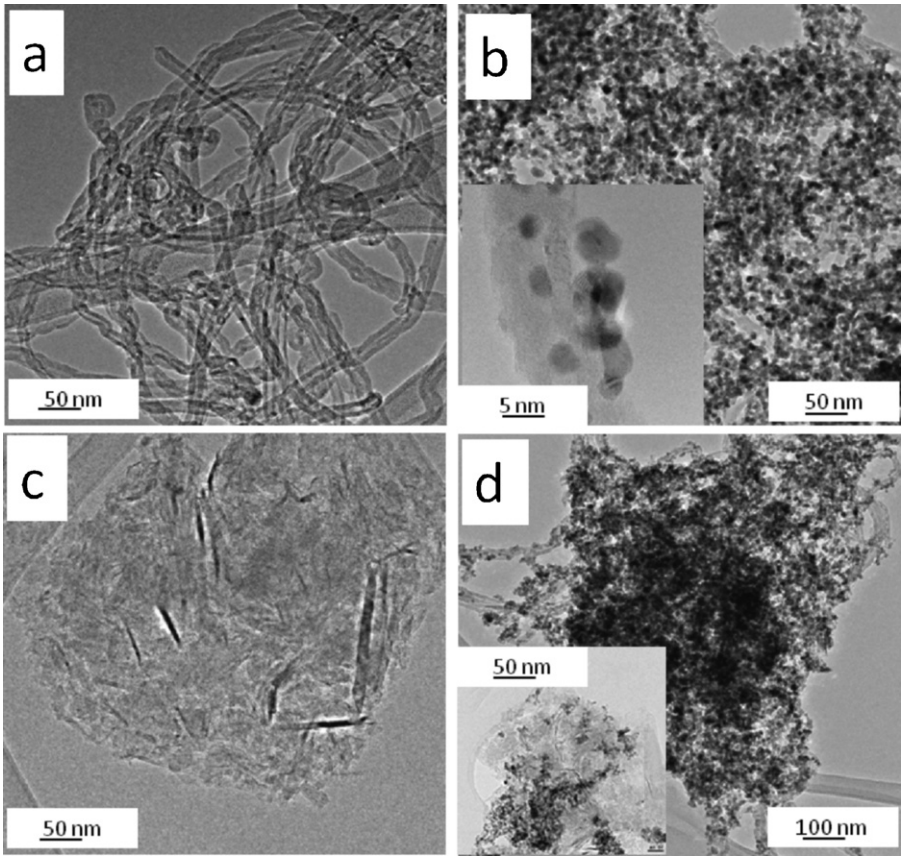

Fig. 4. TEM images of (a) MWCNTs, (b) SnO_2–MWCNTs (inset shows HRTEM image), (c) GNs and (d) GNs/SnO_2–MWCNTs composite.

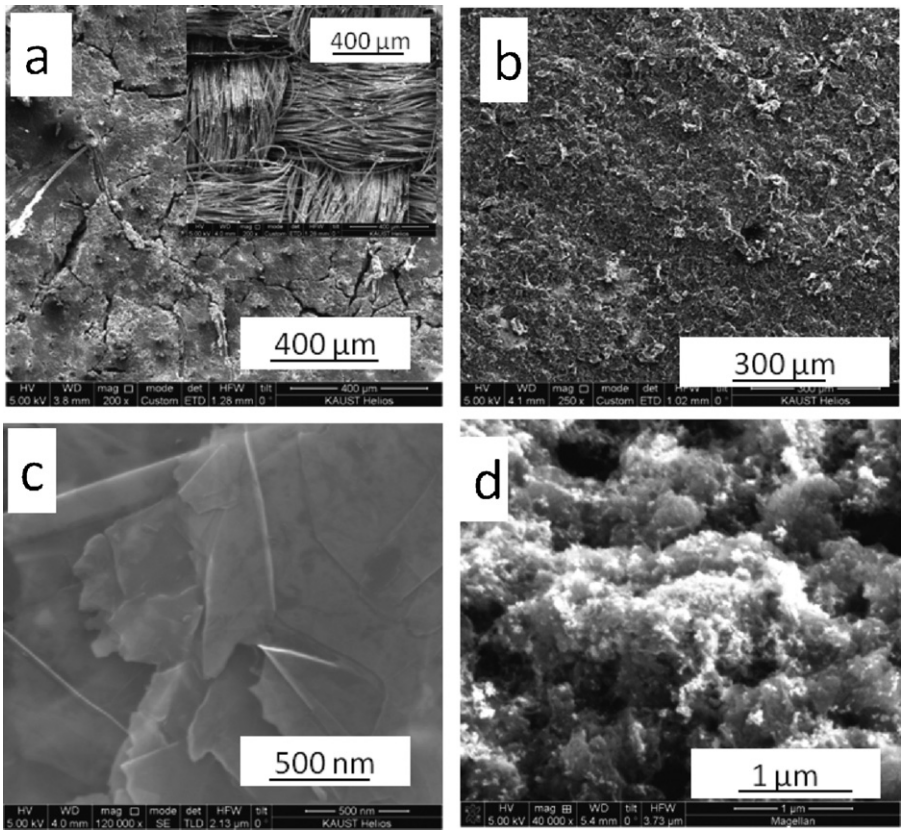

Fig. 5. SEM images of (a) Carbon graphitized cloth substrate (inset shows the back side) (b) and (c) GNs and (d) GNs/SnO_2–MWCNTs composite on graphitized carbon cloth.

are characteristics for supercapacitors with low contact resistance, up to a scan rate of 50 mV s^{-1} indicating an excellent capacitance behavior and low contact resistance. Absence of any oxidation or reduction peaks in the CV loops denotes that pseudocapacitance contribution from SnO_2 nanoparticles to the total capacitance of the GNs/SnO_2–MWCNTs composite based symmetric supercapacitor device is negligibly small. A comparison of CV loops of carbon cloth substrate, GNs and GNs/MWCNTs/SnO_2 composite based supercapacitors at a scan rate of 20 mV s^{-1} is shown in Fig. 6(c). The CV loops of GNs and GNs/SnO_2–MWCNTs symmetric supercapacitors are nearly rectangular in nature. GNs/SnO_2–MWCNTs composite materials show higher capacitive performance than GNs as supercapacitor electrodes. The specific capacitances of GNs and GNs/SnO_2–MWCNTs symmetric supercapacitors obtained from CV loops are 150 and 218 F g^{-1} respectively (using Eqs. (1) and (3)). From Fig. 6(c), it is also evident that the capacitive contribution from the carbon cloth substrate to the electrodes is negligibly small.

Fig. 7 shows the variation in the specific capacitance as a function of scan rates. It can be seen that the specific capacitance decreases with an increase in scan rates from 5 to 200 mV s^{-1}. It is also observed that the specific capacitance of GNs/SnO_2–MWCNTs supercapacitors is much higher than that of GNS based supercapacitor at the same scan rate.

Galvanostatic charge–discharge curves of GNs and GNs/SnO_2–MWCNTs symmetric supercapacitors at a constant current of 5 mA in the potential range between 0 and +1 V are shown in Fig. 8. Charge–discharge measurements are critical in the analysis and prediction of the active materials performance under practical operating conditions. It can be seen that the curves are nearly linear and symmetrical, which is another typical characteristic of an ideal capacitor. Voltage (IR) drop is observed to be very small, which indicates that the electrodes have low internal resistance. In addition, the charge–discharge duration for GNs/SnO_2–MWCNTs composite is greater than that of GNs, indicating a high specific capacitance of 224 F g^{-1} (using Eqs. (2) and (3)) for GNs/SnO_2–MWCNTs composite. For GNs based supercapacitor, the specific capacitance is obtained as 153 F g^{-1}. Specific capacitances at constant currents from 10 to 50 mA are also calculated, however, the results remain practically invariant. The maximum storage energy (E) per unit mass for GNs and GNs/SnO_2–MWCNTs symmetric supercapacitors are calculated as 21.3 and 31.1 Wh kg^{-1} respectively, using Eq. (5)

$$E = \frac{1}{2} C_{sp} V_i^2 \tag{5}$$

where C_{sp} is the specific capacitance and V_i is the initial voltage (1.0 V) of the discharge curve [36].

For practical applications, supercapacitors must have long-term cycle stability. The stability of the supercapacitor devices is evaluated by conducting galvanostatic charge–discharge measurements for 6000 cycles at a constant current of 10 mA in the potential range between 0 and +1 V. Specific capacitance is calculated after a set of 100 cycles. The specific capacitance as a function of cycle number is presented in Fig. 9. Both GNs and GNs/SnO_2–MWCNTs symmetric supercapacitors are found to exhibit excellent cycle life over the entire cycle numbers. After 6000 cycles, GNs and GNs/SnO_2–MWCNTs symmetric supercapacitors retain 92% and 81%, respectively, of their initial specific capacitance indicating that both the electrode materials have got excellent cycle stability and very high degree of reversibility in the repetitive charge–discharge cycling.

Nyquist plots of the GNs and GNs/SnO_2–MWCNTs symmetric supercapacitors are shown in Fig. 10. Plots show a semicircle in the high frequency region and a straight line in the low-frequency region. The high frequency arc is related to the electronic resistance within the electrode materials. The line at the low frequency

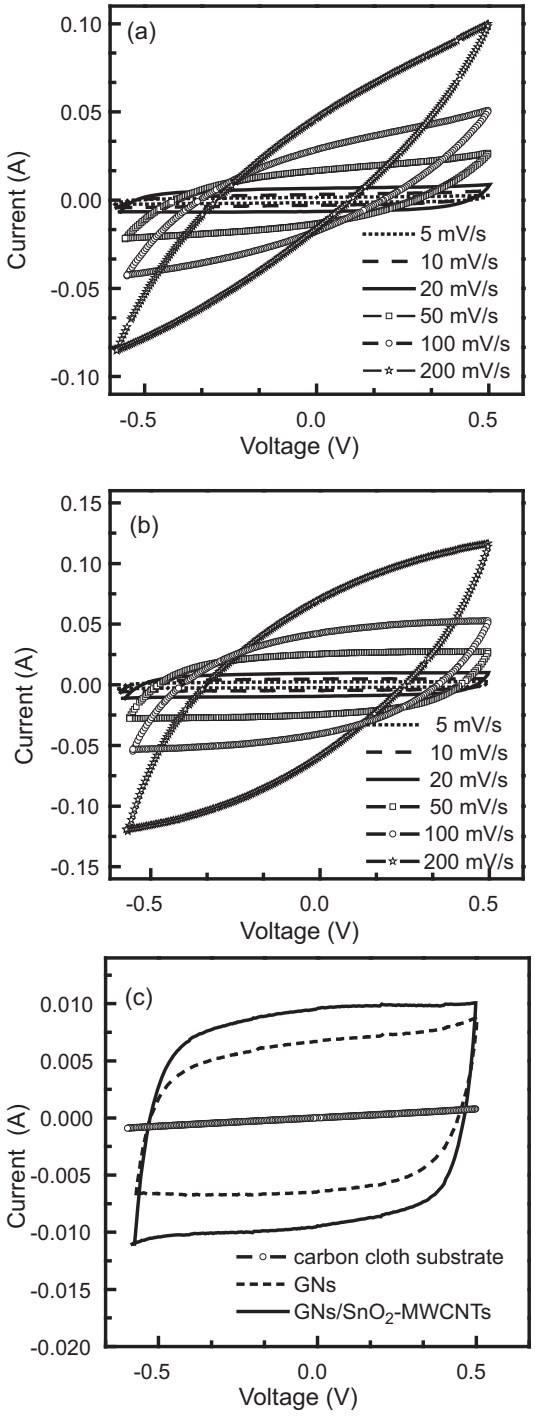

Fig. 6. Cyclic voltammograms of (a) GNs and (b) GNs/SnO_2–MWCNTs composite based supercapacitor devices with various scan rates in the range of −0.6 to +0.5 V and (C) comparison of cyclic voltammograms of carbon cloth substrate, GNs and GNs/SnO_2–MWCNTs composite based supercapacitor devices with scan rate of 20 mV s^{-1}.

region making an angle 45° with the real axis, the Warburg line and is a result of the frequency dependence of ion diffusion in the electrolyte to the electrode interface. The vertical line at lower frequencies parallel to the imaginary axis indicates an ideal behavior, representative of the ion diffusion in the structure of the electrode. The magnitude of equivalent series resistance (ESR) (2.5 Ω and 1.86 Ω respectively for GNs and GNs/SnO_2–MWCNTs composite based electrodes) is obtained from the *x*-intercept of the Nyquist plot in Fig. 9. ESR data is an important factor in determining the

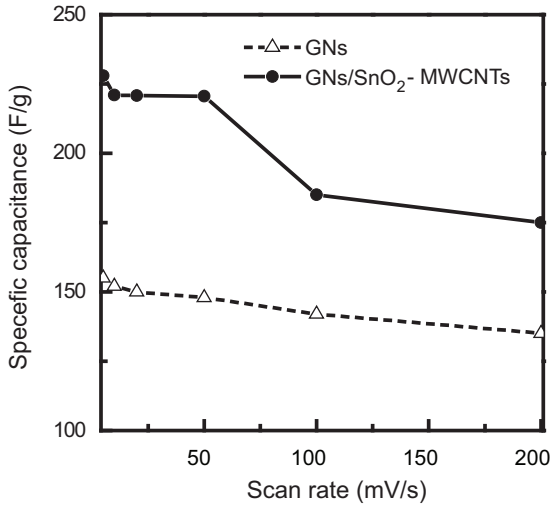

Fig. 7. The specific capacitance change as a function of scan rate.

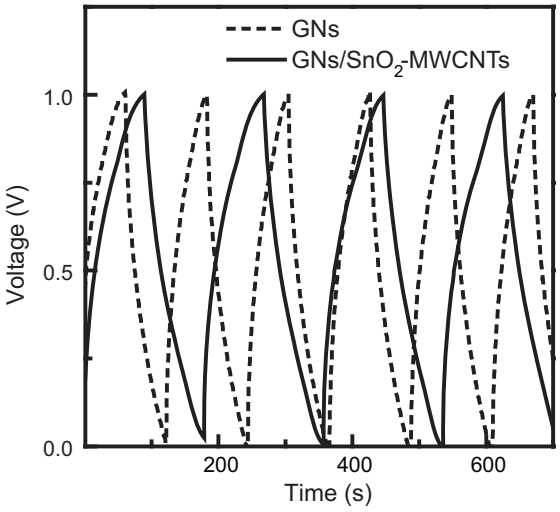

Fig. 8. Galvanostatic charge–discharge curves of GNs and GNs/SnO_2–MWCNTs composite based supercapacitor devices at a constant current density of 5 mA, in 30 wt% KOH electrolyte.

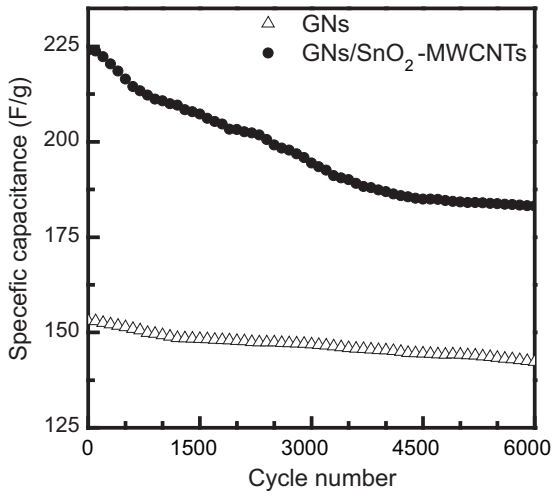

Fig. 9. The specific capacitance change at a constant current of 10 mA as a function of cycle number.

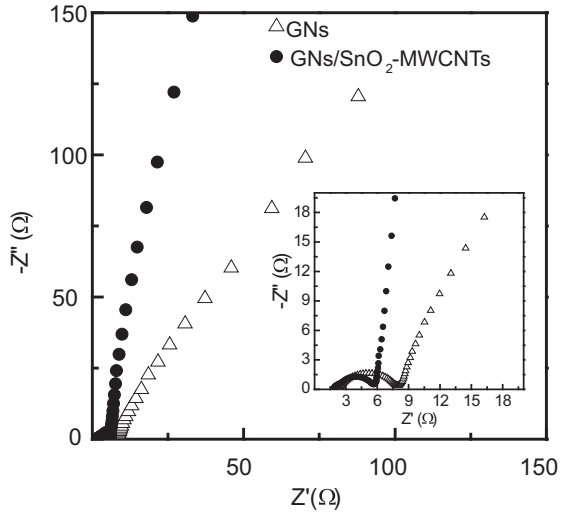

Fig. 10. Nyquist plots for GNs and GNs/SnO_2–MWCNTs composite based supercapacitor devices with the at a dc bias of 0 V with sinusoidal signal of 10 mV over the frequency range from 100 kHz and 1 MHz. Z': real impedance. Z'': imaginary impedance. Inset shows an enlarged scale.

power density of a supercapacitor. The reduction in the ESR value for GNs/SnO_2–MWCNTs composite indicates that SnO_2–MWCNTs provide diffusion path between sheets and improves charge transfer performance of GNs.

The maximum power density (P_{max}) of the supercapacitor devices are calculated from the low frequency data of the impedance spectra, according to Eq. (6)

$$P_{max} = \frac{V_i^2}{4MR} \quad (6)$$

where V_i is the initial voltage (here it is 1 V), R is the ESR and M is the total mass of active materials in two electrodes (in this case 8 mg) with a cell voltage of 1.0 V [36]. Maximum power densities of 12.5 and 17.6 kW kg^{-1} are obtained respectively for GNs and GNs/SnO_2–MWCNTs composite based supercapacitors. This value of power density is well-suited for surge-power delivery applications [36].

Specific capacitance value obtained for chemically modified GNs based supercapacitor in the present study is comparable to that reported by Liu et al. for curved GNs based supercapacitors (154.1 F g^{-1} at 1 A g^{-1}) with ionic electrolyte, but the energy density value is much lower as in the present study, with aqueous KOH electrolyte, the maximum possible potential is less than 1.2 V [6]. For CB spacer dispersed GNs supercapacitor electrodes, a maximum specific capacitance of 175 F g^{-1} has been reported in 6 M aqueous KOH electrolyte [13]. Use of CNT spacers in polymer modified GNs reported to give an average specific capacitance of 120 F g^{-1} in 1 M H_2SO_4 electrolyte [12] and a specific capacitance of 38.9 F g^{-1} has been obtained for SnO_2 nanoparticle coated GNs supercapacitor electrodes [27]. Supercapacitor performance of the GNs/SnO_2–MWCNTs composite we report here is superior to GNs/CB, GNs/CNTs or GNs/SnO_2 composites [12,13,27]. Even though, their performance is found to be inferior to that of conducting polymer dispersed GNs (C_{sp} > 480 F g^{-1}) [14,15,23], they possess excellent cycling stability, which make them suitable for practical applications. Hence, GNs/SnO_2–MWCNTs composite with a maximum specific capacitance of 224 F g^{-1}, energy density of 31.1 Wh kg^{-1} and power density of 17 kW kg^{-1} can be considered as a suitable and promising electrode material for high performance supercapacitors.

4. Conclusions

Symmetric supercapacitor devices were fabricated using GNs and GNs/SnO_2–MWCNTs composite electrodes. The latter gave remarkable results with a maximum specific capacitance of 224 F g^{-1}, power density of 17.6 kW kg^{-1} and an energy density of 31 Wh kg^{-1}. Dispersion of metal oxide loaded MWCNTs helped in the improvement of the capacitance properties of GNs. The fabricated supercapacitor device exhibited excellent cycle life with ~81% of the initial specific capacitance retained after 6000 cycles. These features make GNs/SnO_2–MWCNTs composite quite a suitable and promising electrode material for efficient supercapacitors.

Acknowledgements

Authors acknowledge the help from Dr. Dongkyu Cha (Research Scientist, Advanced Nanofabrication, Imaging & Characterization Lab, KAUST) in TEM and SEM measurements.

References

[1] B.E. Conway, Electrochemical Supercapacitors: Scientific Fundamentals and Technological Applications, Kluwer Academic/Plenum, New York, 1999.
[2] P. Simon, Y. Gogotsi, Nature Materials 7 (2008) 845–854.
[3] M. Jayalakshmi, K. Balasubramanian, International Journal of Electrochemical Science 3 (2008) 1196–1217.
[4] Y. Zhang, H. Feng, X.B. Wu, L.Z. Wang, A.Q. Zhang, T.C. Xia, H.C. Dong, X.F. Li, L.S. Zhang, International Journal of Hydrogen Energy 34 (2009) 4889–4899.
[5] L.L. Zhang, R. Zhou, X.S. Zhao, Journal of Materials Chemistry 20 (2010) 5983–5992.
[6] C.G. Liu, Z.N. Yu, D. Neff, A. Zhamu, B.Z. Jang, Nano Letters 10 (2010) 4863–4868.
[7] K.S. Novoselov, A.K. Geim, S.V. Morozov, D. Jiang, Y. Zhang, S.V. Dubonos, I.V. Grigorieva, A.A. Firsov, Science 306 (2004) 666–669.
[8] A.K. Geim, K.S. Novoselov, Nature Materials 6 (2007) 183–191.
[9] S.R.C. Vivekchand, C.S. Rout, K.S. Subrahmanyam, A. Govindaraj, C.N.R. Rao, Journal of Chemical Sciences 120 (2008) 9–13.
[10] M.D. Stoller, S.J. Park, Y.W. Zhu, J.H. An, R.S. Ruoff, Nano Letters 8 (2008) 3498–3502.
[11] Y. Chen, X. Zhang, P. Yu, Y.W. Ma, Journal of Power Sources 195 (2010) 3031–3035.
[12] D.S. Yu, L.M. Dai, Journal of Physical Chemistry Letters 1 (2010) 467–470.
[13] J. Yan, T. Wei, B. Shao, F.Q. Ma, Z.J. Fan, M.L. Zhang, C. Zheng, Y.C. Shang, W.Z. Qian, F. Wei, Carbon 48 (2010) 1731–1737.
[14] J. Yan, T. Wei, B. Shao, Z.J. Fan, W.Z. Qian, M.L. Zhang, F. Wei, Carbon 48 (2010) 487–493.
[15] K. Zhang, L.L. Zhang, X.S. Zhao, J.S. Wu, Chemistry of Materials 22 (2010) 1392–1401.
[16] C.M. Niu, E.K. Sichel, R. Hoch, D. Moy, H. Tennent, Applied Physics Letters 70 (1997) 1480–1482.
[17] M. Pasta, F. La Mantia, L.B. Hu, H.D. Deshazer, Y. Cui, Nano Research 3 (2010) 452–458.
[18] J.S. Ye, H.F. Cui, X. Liu, T.M. Lim, W.D. Zhang, F.S. Sheu, Small 1 (2005) 560–565.
[19] A.L.M. Reddy, S. Ramaprabhu, Journal of Physical Chemistry C 111 (2007) 7727–7734.
[20] M.C. Henstridge, E.J.F. Dickinson, R.G. Compton, Chemical Physics Letters 485 (2010) 167–170.
[21] Z.J. Fan, J. Yan, L.J. Zhi, Q. Zhang, T. Wei, J. Feng, M.L. Zhang, W.Z. Qian, F. Wei, Advanced Materials 22 (2010) 3723.
[22] E. Yoo, J. Kim, E. Hosono, H. Zhou, T. Kudo, I. Honma, Nano Letters 8 (2008) 2277–2282.
[23] J. Yan, T. Wei, Z.J. Fan, W.Z. Qian, M.L. Zhang, X.D. Shen, F. Wei, Journal of Power Sources 195 (2010) 3041–3045.
[24] Z.S. Wu, D.W. Wang, W. Ren, J. Zhao, G. Zhou, F. Li, H.M. Cheng, Advanced Functional Materials 20 (2010) 3595–3602.
[25] J. Yan, Z.J. Fan, T. Wei, W.Z. Qian, M.L. Zhang, F. Wei, Carbon 48 (2010) 3825–3833.
[26] F.H. Li, J.F. Song, H.F. Yang, S.Y. Gan, Q.X. Zhang, D.X. Han, A. Ivaska, L. Niu, Nanotechnology 20 (2009).
[27] T. Lu, Y.P. Zhang, H.B. Li, L.K. Pan, Y.L. Li, Z. Sun, Electrochimica Acta 55 (2010) 4170–4173.
[28] G.H. Lu, K.L. Huebner, L.E. Ocola, M. Gajdardziska-Josifovska, J.H. Chen, Journal of Nanomaterials (2006).
[29] S. de Monredon, A. Cellot, F. Ribot, C. Sanchez, L. Armelao, L. Gueneau, L. Delattre, Journal of Materials Chemistry 12 (2002) 2396–2400.
[30] X.S.H.T. Fang, L.H. Qian, D.W. Wang, F. Li, Y. Chu, F.P. Wang, H.M. Cheng, Journal of Physical Chemistry C 112 (2008) 5790–5794.

[31] V. Juttukonda, R.L. Paddock, J.E. Raymond, D. Denomme, A.E. Richardson, L.E. Slusher, B.D. Fahlman, Journal of the American Chemical Society 128 (2006) 420–421.
[32] H. Kim, S.W. Kim, Y.U. Park, H. Gwon, D.H. Seo, Y. Kim, K. Kang, Nano Research 3 (2010) 813–821.
[33] E.D. Grayfer, A.S. Nazarov, V.G. Makotchenko, S.J. Kim, V.E. Fedorov, Journal of Materials Chemistry 21 (2011) 3410–3414.
[34] V. Khomenko, E. Frackowiak, F. Beguin, Electrochimica Acta 50 (2005) 2499–2506.
[35] A. Dieguez, A. Romano-Rodriguez, A. Vila, J.R. Morante, Journal of Applied Physics 90 (2001) 1550–1557.
[36] Y. Wang, Z.Q. Shi, Y. Huang, Y.F. Ma, C.Y. Wang, M.M. Chen, Y.S. Chen, Journal of Physical Chemistry C 113 (2009) 13103–13107.